

## Comparative Analysis of Aerodynamic Characteristics of Rectangular and Curved Leading Edge Wing Planforms

Md. Monirul Islam Khan, Abdullah Al-Faruk

Department of Mechanical Engineering, Khulna University of Engineering & Technology, Bangladesh

Corresponding Author: Abdullah Al-Faruk

**ABSTRACT:** Shape of aircraft wing, which is the lifting surface with the chosen airfoil sections, is crucial to the aircraft performance. The performance of an aircraft mostly depends on the aerodynamic characteristics of wings, such as, lift and drag coefficients, lift to drag ratio etc. This work numerically investigates the aerodynamic performance of NACA 2412 airfoil wing by incorporating curvature at the leading edge. Two wing models: rectangular planform with straight leading and trailing edges, and curved leading edge with straight trailing edge were simulated using commercial CFD package ANSYS fluent keeping equal span length and surface area. Both models were analyzed at an air velocity of 100 m/s (Reynolds number 617,000 based on chord length). The lift and drag forces at 0°, 4°, 8°, 12°, 16°, and 20° angles of attack were determined and the lift coefficient, drag coefficient and lift to drag ratio were analyzed. The result shows that, the curved leading edge wing planform have higher lift coefficient and lower drag coefficient than the rectangular wing planform. Consequently, the curved leading edge planform have higher lift to drag ratio than the rectangular planform.

**KEYWORDS-** Curved wing planform, Drag coefficient, Lift coefficient, Lift to drag ratio, NACA 2412 airfoil

Date of Submission: 27-04-2018

Date of acceptance: 12-05-2018

### I INTRODUCTION

An airfoil is perpendicular cross-section of a wing, or the blade of a propeller, rotor, turbine etc. An aerodynamic force is produced when an airfoil-shaped object moved through a fluid. The lift on an airfoil is primarily due to the result of its shape and angle of attack with the freestream relative wind direction. When a fixed-wing aircraft is oriented at a suitable angle, the airfoil deflects the oncoming air downward, resulting a force on the airfoil in the direction opposite to the deflection. This force is known as aerodynamic force and can be resolved into two components: lift and drag. The component perpendicular to the direction of motion is called lift whereas the component parallel to the direction of motion is called drag [1]. Most airfoil shape require a positive angle of attack to generate the lift, but cambered airfoils can generate lift at zero angle of attack. The turning of the air in the vicinity of the airfoil creates curved streamlines, resulting in lower pressure on upper side and higher pressure on lower side of the airfoil. The pressure difference accompanied by a velocity difference, via the Bernoulli's principle, so the resulting flow field around the airfoil has a higher average velocity on the upper surface than the lower surface. The lift force can be related directly to the average top/bottom velocity difference without computing the pressure by using the concept of circulation and the Kutta-Joukowski theorem [2].

Similar to a bird's wing, an aircraft wing is the lifting surface with the chosen airfoil section, whose shape/geometry can be varied span wise to search better performance. The lift generated by the wing sustains the weight of the aircraft to make flight in the air. Again, from an aerodynamic perspective, the main source of the airplane drag is associated with the wing. Around two-thirds of the total drag of typical transport aircraft at cruise conditions is produced by the wing [3]. Therefore, the effects of wing shape and size are critical to the aerodynamic characteristics (e.g., lift, drag, lift to drag ratio etc.) consequently the performance of the airplane. As such, research on different wing shapes/geometries are still on throughout the world to explore the maximum possible lift and minimum possible drag. Hossain et al. conducted an experimental analysis for the aerodynamic characteristics of rectangular wing with and without bird feather-like winglets for different Reynolds Number [4]. The result shows a 25~30% reduction in drag coefficient and 10~20% increase in lift coefficient using the bird

feather like winglet at  $8^\circ$  angle of attack. Dwivedi et al. adopted a simple approach for experiment on aerodynamic static stability analysis of different types of wing shapes [5]. They tested the reduced scale size wings of different shapes like rectangular, rectangular with curved tip, tapered, tapered with curved tip, etc. in low speed subsonic wind tunnel at different air speeds and different angles of attack. The authors found that the tapered wing with curved tip was the most stable at different speeds and ranges of working angles of attack. Mineck and Vijjen tested three planar, untwisted wings with the same elliptical chord but with different curvatures of the quarter-chord line [6]. They found that the elliptical wing with the unswept quarter-chord line has the lowest lifting efficiency, the elliptical wing with the unswept trailing edge has the highest lifting efficiency and the crescent-shaped wing has efficiency in between. Recktenwald tested a circular planform non-spinning body with an airfoil section and compared with Cessna 172 model [7]. The author found that the lift curve slope was less than that of Cessna 172 but displayed better stall characteristics. Wakayama studied and presented basic results from wing planform optimization for minimum drag with constraints on structural weight and maximum lift [8].

Aerodynamic characteristics analysis for different airfoils have also been conducted at different parts of the world like Mahmud [9] analyzed the effectiveness of an airfoil with bi-camber surface, Kandwal and Singh [10] studied the fluid flow and aerodynamic forces on an airfoil, Robert [11] studied the variation of pressure distribution over an airfoil with Reynolds number, Sharma [12] analyzed the flow behavior around an airfoil body, etc. Researches on different airfoils and conventional wing geometries like rectangular, sweepback, tapered or, delta shapes have also been carried out in many places around the world in an extensive way. However, aerodynamic characteristics of curved-edge wing geometries are yet to be explored numerically to observe the flow field around the wing. In the present work, numerical investigations are carried out to investigate the aerodynamic characteristics of curved leading edge wing. Two geometries of NACA 2412 airfoil with rectangular planform and with curved leading edge planform are developed in Solidworks to compare numerically in ANSYS Fluent. The lift and drag coefficients are determined and compared for both models. Moreover, the flow characteristics around the models are analyzed through visualizing the pressure and velocity contours, and the velocity streamlines.

## II METHODOLOGY OF NUMERICAL MODEL

The methodology of numerical modeling is one of important part which requires lot of steps to achieve the research objectives. This section will explain the tools used for the CFD simulations. CFD performs its required analysis with the help of three basic elements: (a) pre-processor, (b) solver, and (c) post-processor.

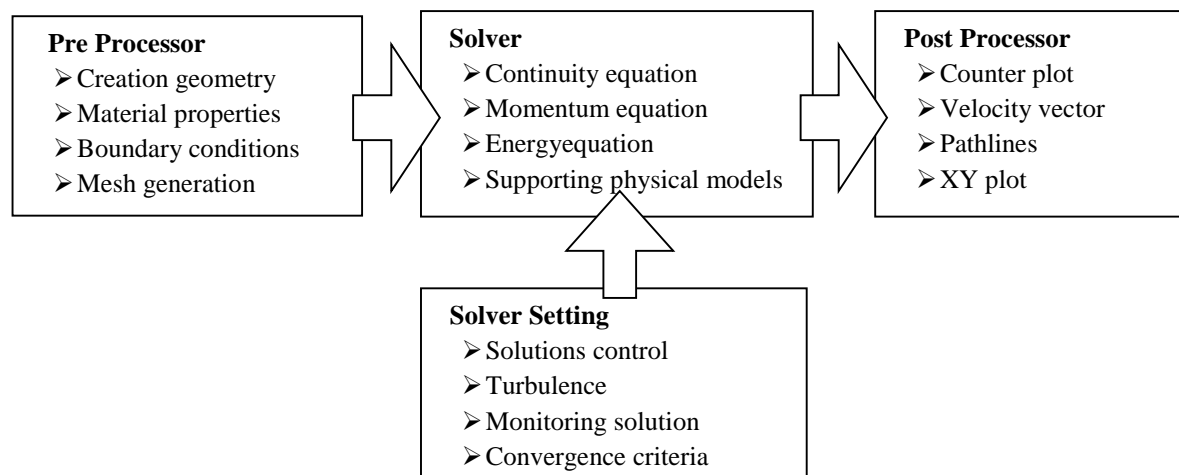


Figure 1: Numerically solving technique of the prototype [13]

Pre-process consists of the creation of geometry, generating a mesh of the geometry, assigning material for the physical model and defining boundary conditions for acquiring realistic data as illustrated in Figure 1. The preprocessed data then provided to the solver for running the simulation process.

The numerical solver is basically a code for calculating a given set of data according to the boundary conditions provided. The fundamental governing equations of fluid dynamics are the continuity, momentum and energy equations. The physics of any fluid flow and heat transfer is governed by these equations. After the solution is initiated, a set of solution control command is provided and the solution is monitored continuously. Every time, when a single iteration is done, the solver checks for the convergence criteria. If the convergence characteristics

are achieved, then it will automatically stop the calculation and if it is not, calculation is modified as in the following line diagram of Figure 2.

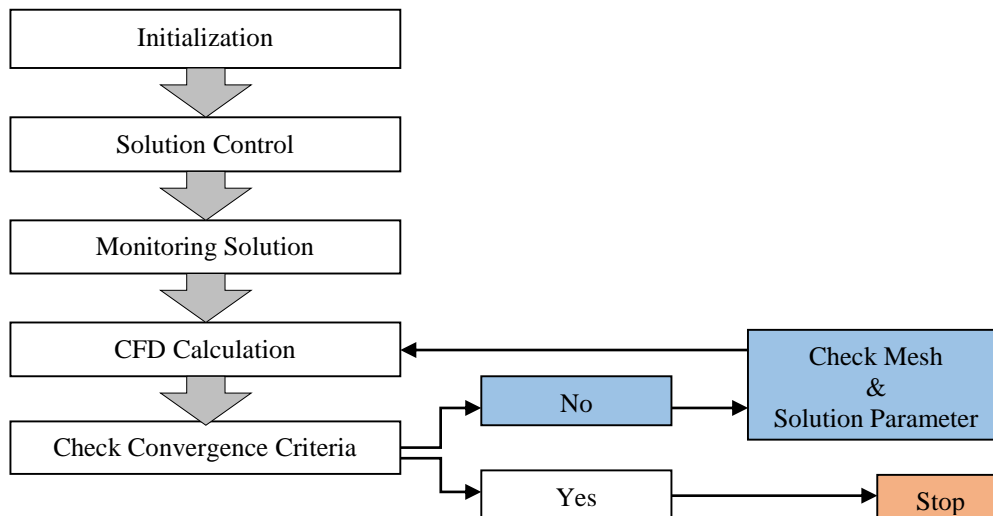


Figure 2: Solver Solution technique [13]

At present, different high-end software are available which has an excellent graphical interface for better visualization of the result such as in the form of color contours, vectors, pathlines, XY plots, graphs etc. The ANSYS fluid dynamics solution is a comprehensive suite of products that allows user to predict the impact of fluid flows on the product throughout design and manufacturing as well as during end use.

**I.1 Geometry development**

Airfoils in subsonic airplanes have a characteristic shape with a rounded leading edge, followed by a sharp trailing edge, often with a symmetric curvature of upper and lower surfaces [14]. Airfoil geometry can be characterized by the coordinates of the upper and lower surface. It is often summarized by a few parameters such as: maximum thickness, maximum camber, position of max thickness, position of max camber, and nose radius, which are shown in Figure 3. One can generate a reasonable airfoil section given these parameters.

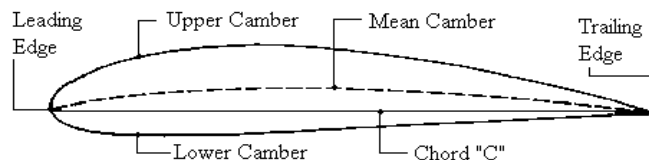


Figure 3: Nomenclature of a typical airfoil section [14]

The NACA airfoil section is created from a camber line and a thickness distribution plotted perpendicular to the camber line. The equation for the camber line is split into sections either side of the point of maximum camber position (P). In order to calculate the position of the final airfoil envelope later the gradient of the camber line is also required. The equations are [15]:

$$\begin{aligned}
 &\text{Front}(0 \leq x \leq P) && \text{Back}(P \leq x \leq 1) \\
 \text{Camber } y_c &= \frac{M}{P^2}(2Px - x^2) && y_c = \frac{M}{(1-P)^2}(1 - 2P + 2Px - x^2) \\
 \text{Gradient } \frac{dy_c}{dx} &= \frac{2M}{P^2}(P - x) && \frac{dy_c}{dx} = \frac{2M}{(1-P)^2}(P - x)
 \end{aligned}$$

The thickness distribution is given by the equation:

$$\begin{aligned}
 y_t &= \frac{T}{0.2}(a_0x^{0.5} + a_1x + a_2x^2 + a_3x^3 + a_4x^4) \\
 \text{where } a_0 &= 0.2969 & a_1 &= -0.126 & a_2 &= -0.3516 & a_3 &= 0.2843 & a_4 &= \\
 & & & & & & & & & -0.1015 \text{ or } -0.1036 \text{ for closed trailing edge}
 \end{aligned}$$

The constants  $a_0$  to  $a_4$  are for a 20% thick airfoil. The expression  $T/0.2$  adjusts the constants to the required thickness. At the trailing edge ( $x = 1$ ) there is a finite thickness of 0.0021 chord width for a 20% airfoil. If a closed trailing edge is required the value of  $a_4$  can be adjusted. The value of  $y_t$  is a half thickness and needs to be applied both sides of the camber line. Using the equations above, for a given value of  $x$  it is possible to calculate the camber line position  $y_c$ , the gradient of the camber line and the thickness. The position of the upper and lower surface can then be calculated perpendicular to the camber line.

$$\theta = \tan^{-1} \left( \frac{dy_c}{dx} \right)$$

Upper Surface  $x_u = x_c - y_t \sin \theta$   $y_u = y_c + y_t \cos \theta$

Lower Surface  $x_l = x_c + y_t \sin \theta$   $y_l = y_c - y_t \cos \theta$

The most obvious way to plot the airfoil is to iterate through equally spaced values of  $x$  calculating the upper and lower surface coordinates. While this works, the points are more widely spaced around the leading edge where the curvature is greatest and flat sections can be seen on the plots. To group the points at the ends of the airfoil sections a cosine spacing is used with uniform increments of  $\beta$  [15].

$$x = \frac{(1 - \cos \beta)}{2} \quad \text{where } 0 \leq \beta \leq \pi$$

Using NACA 2412 airfoil, a rectangular wing model and a curved leading edge wing models are drawn in Solidworks 13 of the same span (200 mm) and surface area as shown in Figure 4. For rectangular wing, the chord length is the same (100 mm) along the span. For the curved leading edge planform cord length varied from (120 mm to 80 mm). For rectangular planform surface area is 41150.52 mm<sup>2</sup> and for curved leading edge surface area is 41172.18 mm<sup>2</sup>.

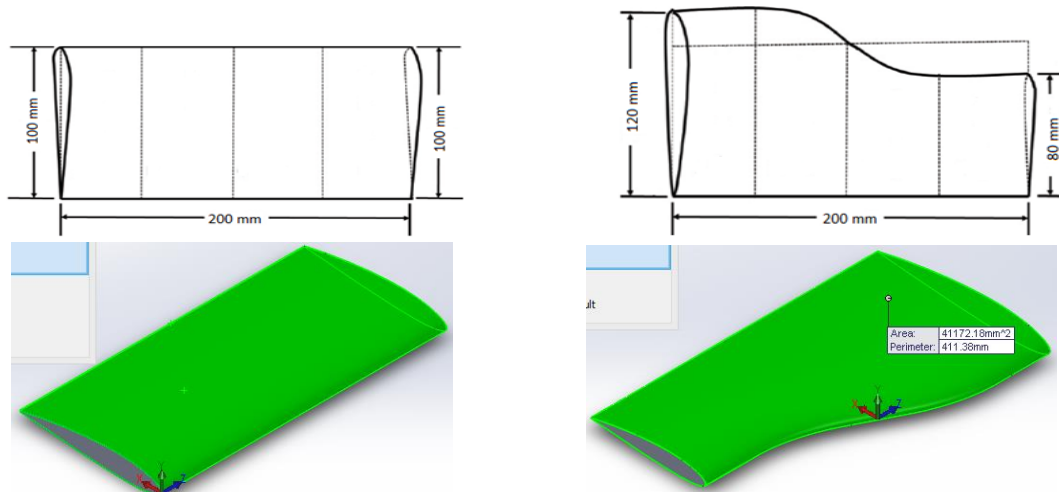


Figure 4: Solidworks design of rectangular planform (left) and curved leading edge planform (right)

Then as an external geometry file the models were exported in ANSYS. Domain was created with the given dimensions as shown in Figure 5. The domain was set as fluid domain where the solid airfoil was subtracted from the domain.

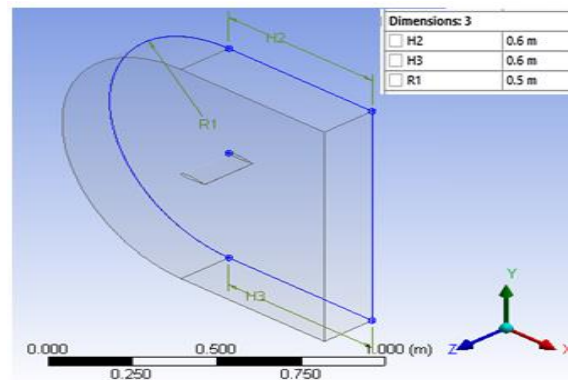


Figure 5: The schematic of computation domain with the geometry in ANSYS

**I.2 Generation of mesh**

ANSYS meshing was used to discretize the computation domain. A set mesh were created with different sizes and nodes for testing the mesh independency of the CFD simulation keeping the same face meshing and mesh sizing. Figure 6 illustrate a photograph of a mesh generated around the airfoil along with the details.

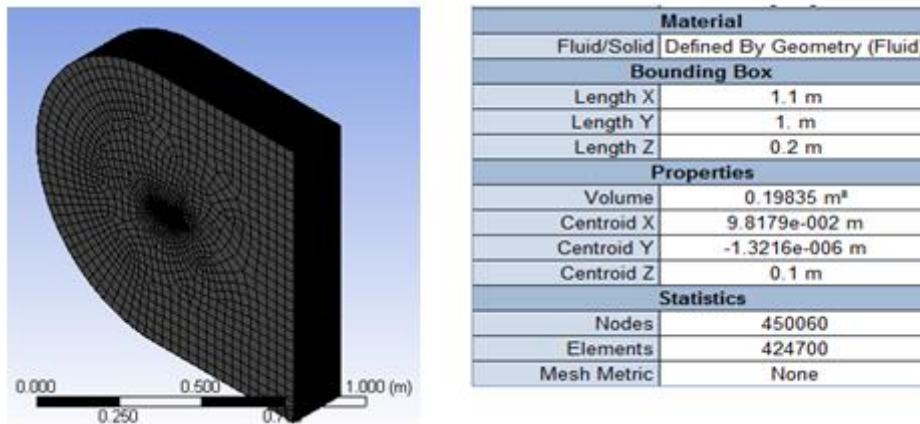


Figure 6: Generated mesh with the details

It is first step in performing a CFD simulation to investigate the effect of the mesh size on the solution results. Generally, a numerical solution becomes more accurate as more nodes are used, but using additional nodes also increases the required computer memory and computational time [13]. The appropriate number of nodes can be determined by increasing the number of nodes until the mesh is sufficiently fine so that further refinement does not change the results. Figure 7 shows the effect of number of grid cells in coefficient of lift at 12° angle of attack. This study revealed that 450060 nodes would be sufficient to establish a mesh independent solution.

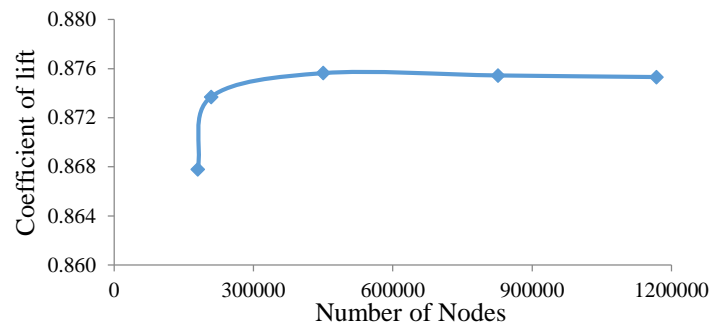


Figure 7: Mesh independency analysis with various element size

**I.3 Boundary conditions**

The domain involves inlet, outlet and wall boundaries as illustrated in Figure 8. Velocity inlet boundary condition was applied at inlet with freestream velocity of 100m/s and the outflow boundary condition was pressure outlet with zero relative pressure. Surfaces of wing were prescribed as slip wall.

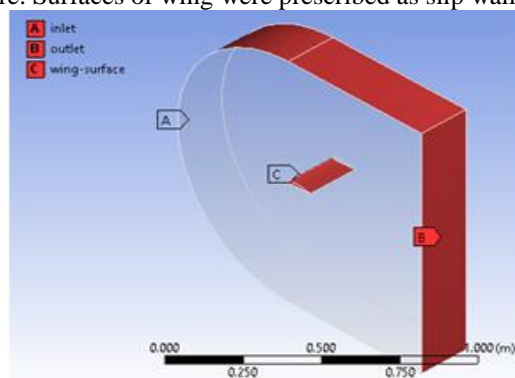


Figure 8: Boundary conditions of the computational domain

For each angle of attack, the velocity components were calculated as follows: the x-component of velocity becomes  $u \cos \alpha$  and the y component of velocity changed by  $u \sin \alpha$ , where  $\alpha$  is the angle of attack in degrees and  $u$  is the relative wind velocity. ANSYS recommends turbulence intensities ranging from 1% to 5% as inlet boundary conditions. In this study it was assumed that inlet velocity is less turbulent than pressure outlet. Hence, for velocity inlet boundary condition turbulence intensity is considered 1% and for pressure outlet boundary 5%. In addition, ANSYS also recommends turbulent viscosity ratio of 10 for better approximation of the problem [16].

**I.4 Simulation setup and solution**

In this study, steady 3-D numerical simulations were carried out with the realizable  $k$ -epsilon turbulence model. The wall was treated as non-equilibrium wall functions. Heat transfer was disabled as assumed that no heat transfer was taken place. The calculation was started by requesting 1000 iterations. In the monitor, wing-surface was selected as the wall zone residuals; lift and drag were monitored. At first solution was initialized from inlet by standard initialization. Reporting interval and profile update interval were both set as 1. Solution was being calculated till it converged as shown one in Figure 9.

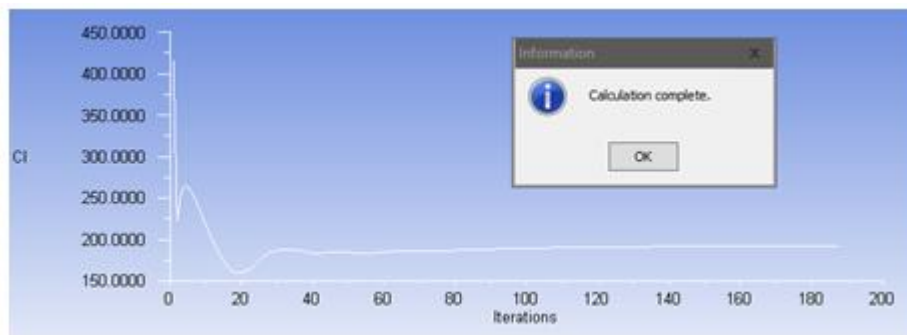


Figure 9: Convergence history of a numerical computation

**II. RESULTS AND DISCUSSION**

**II.1 Aerodynamic performance analysis**

The pressure and shear stress distribution around the wing surface area are the main source of lift and drag of the airplane [14]. The lift and drag forces for both curved and rectangular profile for different angles of attack were found from the post-processor once the simulation were converged. Then coefficient of lift and drag were calculated from the lift force and drag force, respectively, utilizing the following relationships

$$F_D = \frac{1}{2} \rho AV^2 C_D \quad F_L = \frac{1}{2} \rho AV^2 C_L$$

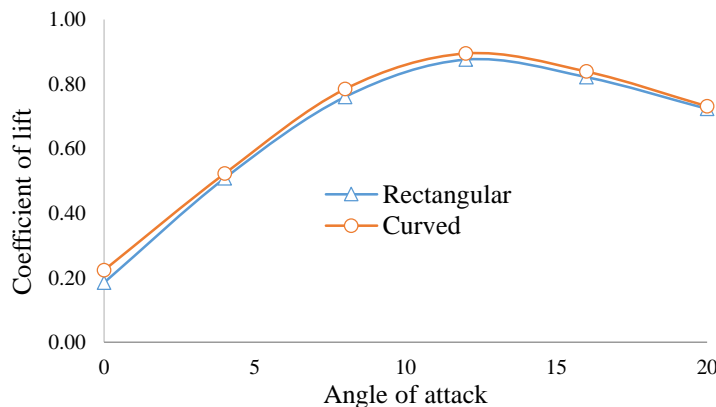


Figure 10: Coefficient of lift versus angle of attack

Variation of lift coefficient at different angle of attack for both the wings is shown below in Figure 10. It is observed that the lift coefficient for curved leading edge wing is higher than the lift coefficient of rectangular

wing at every angle of attack. However, greater values of lift coefficient are observed at 0°, 8° and 12° angles. The stall angle of attack for both the wings remains within the same at 12° where the lift coefficients are decreasing.

The variation of drag coefficient for both the wings are plotted against different angles of attack in Figure 11 and it is observed that the values of drag coefficient for curved leading edge wing is lower than that of the rectangular wing. Prominent reduction in drag coefficient values for curved leading edge wing is found at 0° and 12° angle of attack.

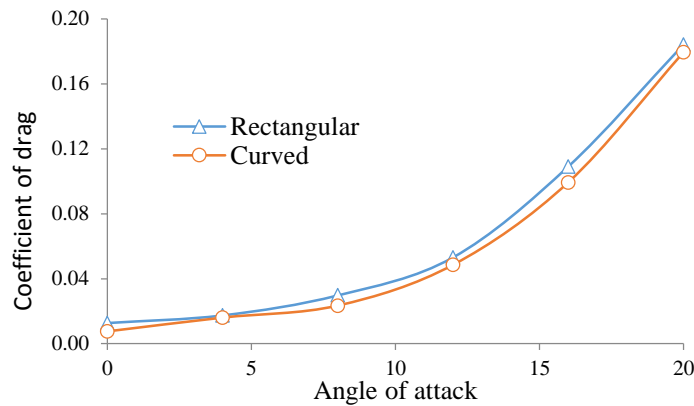


Figure 11: Coefficient of drag against the angle of attack

The values of lift to drag ratio are plotted for various angles of attack below in Figure 12 and it shows that the lift to drag ratio of curved leading edge wing is higher than that of the rectangular wing. It is also observed that curved leading edge planform can provide higher lift to drag ratio than the rectangular planform at angles of attack below 12°.

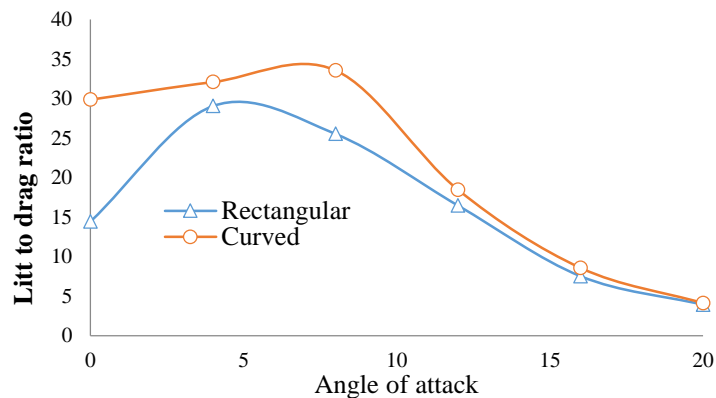
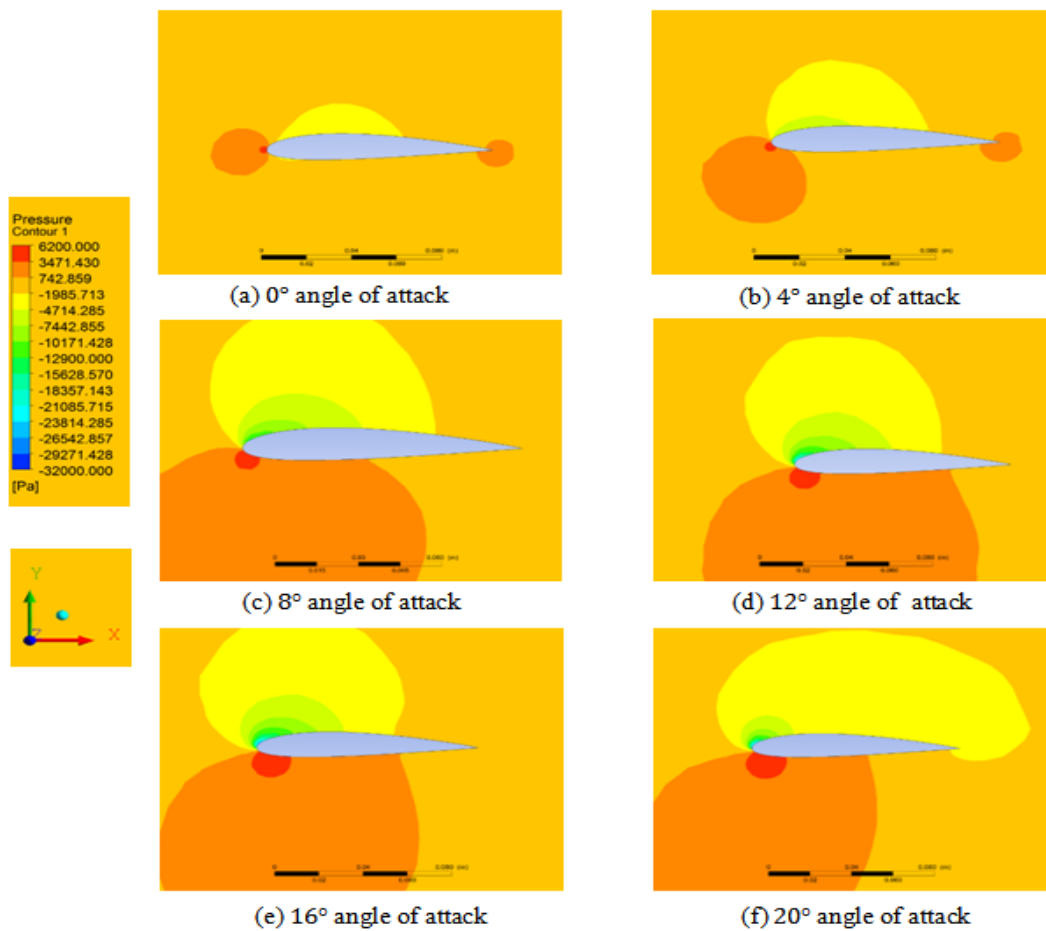


Figure 12: Variation of lift to drag ratio with angle of attack

**II.2 Flow field analysis**

The variation of pressure can be visualized by the pressure contours. Pressure at higher surface is negative and positive at upper surface. Due to negative pressure at upper surface and positive pressure at lower surface lift occurs. Pressure increases at lower surface with the increase of angle of attack till the stall angle of attack as shown in Figure 13. Thus at higher angle of attack lift is high. After the stall angle of attack pressure decreases at lower surface and thus lifts decreases again as shown in Figure 10.



**Figure 13: Contour of pressure at different angle of attack**

Variation of velocity at upper surface and lower surface can be visualized by velocity contours of Figure 14. Velocity at upper surface is higher than lower surface. The lifting phenomenon can also be explained using the Bernoulli's equation. According to Bernoulli's equation, for an incompressible steady state flow, pressure increases if the flow velocity decreases and vice versa. When the air passes over the airfoil, velocity increases as the air continues to flow from its leading edge to the upper surface of the airfoil. The pressure is decreased in that area. But on the other hand, velocity decreases as the air passes through the bottom of the airfoil and the pressure is increased. This positive pressure acting upward acts as the key ingredient for generating lift.

Velocity streamlines for different angles of attack are shown in Figure 15 below. The line indicates the flow directions. Velocity increases at upper surface with the increase in angle of attack. After the critical angle of attack velocity decreases at upper surface. After the critical angle flow separates which are clearly visible by the velocity contours in Figure 14 and velocity streamlines of Figure 15. Due to this flow separation lift reduces after critical angle of attack. Vortex also created at trailing edge at high angle of attack.

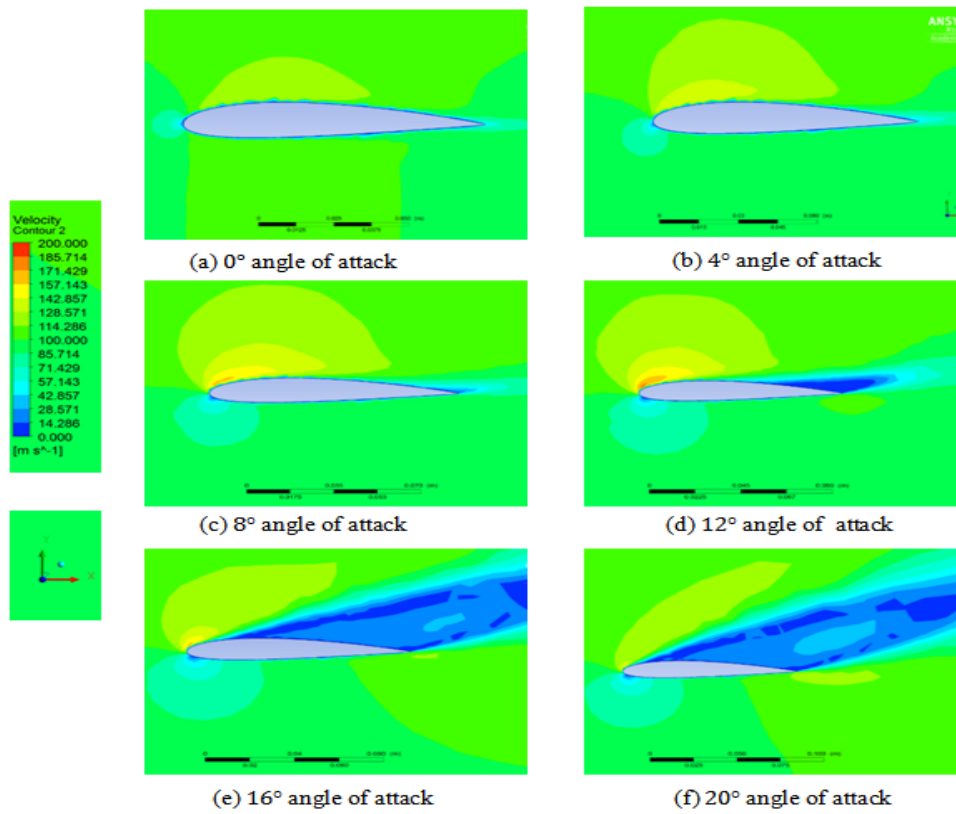


Figure 14: Velocity contour of flow over airfoil at different angle of attack

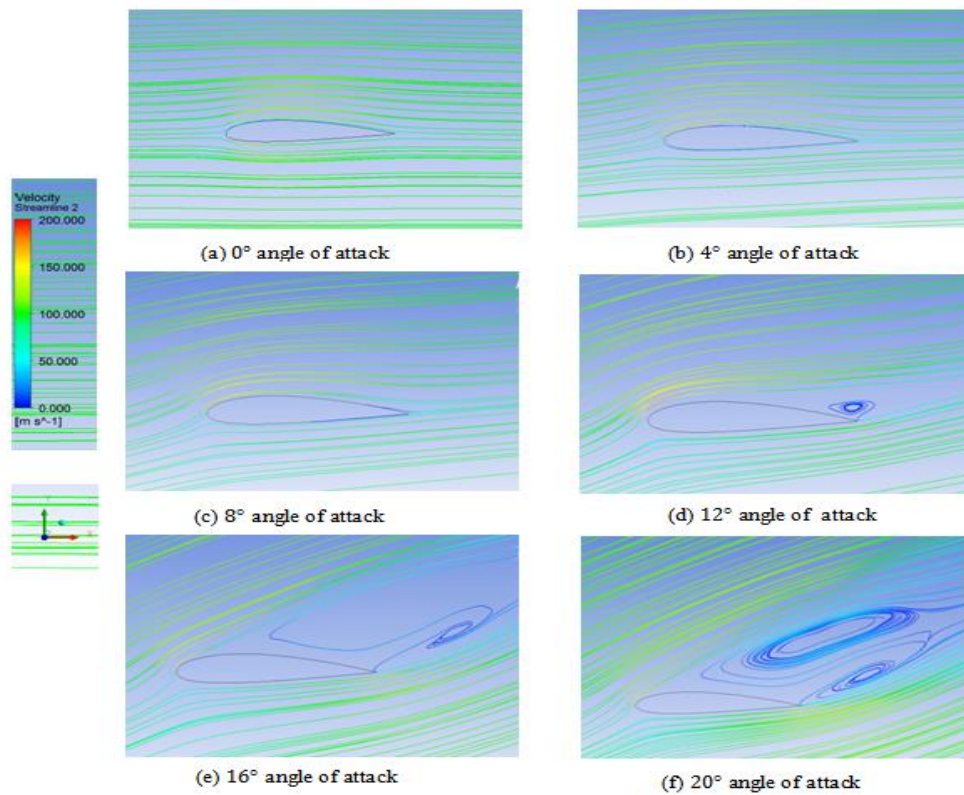


Figure 15: Velocity streamlines over airfoil at different angle of attack

### III. CONCLUSIONS

In this work, curvature was incorporated at the leading edge in such a way that the surface area from the middle of the wing towards the root increases and towards the tip the area decreases in the same rate. The overall surface area of the curved wing planform remains the same as of the rectangular planform. As a result, the wing can produce more lift due to increased surface area near the root. At the same time, flow separation along the span of the wing is reduced due to gradual reduction of chord length along the span and so the drag is also reduced. It is observed that stall angle of attack does not vary significantly between the two wing planforms. Beyond the stall angle of attack, lift and drag coefficients values are almost equal. Therefore, it can be concluded that the curved leading edge planform exhibits better aerodynamic performance than the rectangular planform due to higher lift to drag ratio at angles of attack.

### REFERENCES

- [1]. J.J. Bertin and R.M. Cummings, *Aerodynamics for engineers* (Essex CM20 2JE, England: Pearson Education Limited, 2014).
- [2]. J.D. Anderson Jr., *Fundamentals of aerodynamics* (1221 Avenue of the Americas, NY 10020: McGraw-Hill Companies, 2011).
- [3]. F.T. Lynch, Commercial transports-aerodynamic design for cruise performance efficiency in transonic aerodynamics, in D. Nixon (Ed.), *Progress in astronautics and aeronautics*, 81 (New York: AIAA, 1982) 81-144.
- [4]. A. Hossain, A. Rahman, A.K.M.P. Iqbal, M. Ariffin, and M. Mazian, Drag analysis of an aircraft wing model with and without bird feather like winglet, *International Journal of Aerospace and Mechanical Engineering*, 6(1), 2012, 8-13.
- [5]. Y.D. Dwivedi, M.S. Prasad and S. Dwivedi, Experimental aerodynamic static stability analysis of different wing planforms, *International Journal of Advancements in Research & Technology*, 2(6), 2013, 60-63.
- [6]. R.E. Mineck, and P.M.H.W. Vijgen, Wind-tunnel investigation of aerodynamic efficiency of three planar elliptical wings with curvature of quarter-chord line, *NASA Technical Paper*, 3359, 1993, 1-20.
- [7]. B. Recktenwald, Aerodynamics of a circular planform aircraft, *American Institute of Aeronautics and Astronautics*, 022308, 2008, 1-7.
- [8]. S. Wakayama, Subsonic wing planform design using multidisciplinary optimization, *Journal of Aircraft*, 32(4), 1995, 746-753.
- [9]. M.S. Mahmud, Analysis of effectiveness of an airfoil with bi-camber surface, *International Journal of Engineering & Technology*, 3(5), 2013, 569-577.
- [10]. S. Kandwal and S. Singh, Computational fluid dynamics study of fluid flow and aerodynamic forces on an airfoil, *International Journal of Engineering & Technology*, 1(7), 2012, 1-8.
- [11]. M.P. Robert, The variation with Reynolds number of pressure distribution over an airfoil section, *NACA Report*, 613, 65-84.
- [12]. A. Sharma, Evaluation of Flow Behavior around an Airfoil Body", Thapar University, Patiala-147004, India, July 2012, pp.1-60.
- [13]. H.K. Versteeg and W. Malalasekera, *An introduction to Computational Fluid Dynamics: The Finite Volume Method* (Essex CM20 2JE, England, Pearson Education, 2007).
- [14]. J.D. Anderson, *Introduction to flight* (USA, McGraw-Hill).
- [15]. Airfoil Tools, <http://airfoiltools.com/>
- [16]. ANSYS, ANSYS CFX-solver modeling guide, USA; 2010.